J6.3

GLOBAL ATMOSPHERIC TEMPERATURE AND HUMIDITY PROFILES BASED ON INTERSATELLITE CALIBRATED HIRS MEASUREMENT

Lei Shi
NOAA/NESDIS/NCDC, Asheville, NC

1. INTRODUCTION

The High Resolution Infrared Radiation Sounder (HIRS) on board the National Oceanic and Atmospheric Administration (NOAA) polar orbiting satellite series has been making routine measurement of the atmosphere for more than thirty years. The HIRS has twenty spectral channels, twelve of which are longwave channels. Among the longwave channels, channels 1-7 are located in the carbon dioxide (CO_2) absorption band for measuring temperatures from near surface to stratosphere. Channel 8 is a window channel for surface temperature observation. Channel 9 is in the ozone band. Channel 10 is in the water vapor continuum band. Channels 11 and 12 are designed for measuring water vapor in the mid- and upper troposphere, respectively.

There have been more than a dozen satellites carrying the HIRS instruments in the NOAA polar orbiting satellite series. Due to the independence in the calibration based on individual HIRS instrument's channel spectral response function along with other factors, biases exist from satellite to satellite. To generate a climate data record, it is important that the intersatellite biases are corrected.

To minimize the intersatellite biases, the current study performs an intersatellite calibration based on simultaneous nadir overpass (SNO) observations. HIRS measurements from the NOAA series of polar orbiting satellites are calibrated to a baseline satellite to form a homogeneous database for deriving atmospheric temperature and humidity profiles.

2. INTERSATELLITE CALIBRATION

The SNOs are the measurements taken at the orbital intersections of each pair of satellites viewing the same earth target within a few seconds ((Cao et al., 2005). These satellite intersections are found in the regions +70° to +80°, and -70° to -80° latitude zones once every 8-9 days. Measurements from HIRS SNOs are examined (Shi et al. 2008). Each HIRS channel has its own variation pattern of the intersatellite biases. The biases for each longwave channel (channels 1-12) from N6 to N17 are shown in Fig. 1. The features observed in each of the channels are discussed below.

* Corresponding author address: Lei Shi, National Climatic Data Center, NOAA/NESDIS, Asheville, NC 28801; e-mail: lei.shi@noaa.gov

***Channel 1*:** The biases for each satellite pairs are generally at or larger than 1 K. The biases reach values of larger than 3 K for several pairs of satellites (including N10-N11, N15-N16, and N16-N17). Overall, channel 1 exhibits largest intersatellite biases compared to other temperature sounding channels. This pattern is consistent with what was found in a past study with respect to spectral response function (SRF) measurement uncertainties in pre-launch (Cao et al. 2004). The study indicated that the uncertainty of channel 1 may include both pre-launch measurement errors and the SRF differences.

***Channel 2*:** The biases for most of the satellite pairs are less than 0.6 K. One exception is the bias between N10 and N11, in which the bias value can be as large as -1.3 K at the low scene temperature.

***Channels 3-6*:** These are the channels located along the sharp transmission line of the infrared spectrum, for sensing the upper and middle tropospheric temperature. More than half of the satellite pairs exhibit significant temperature dependent variations of larger than 0.5 K. If this temperature-dependent bias variation feature is not considered properly in the long-term intersatellite calibration, the errors can be carried onto the derived products such as temperature, water vapor, and cloud properties.

***Channel 7*:** This is another channel that is located at the sharp transmission line of the infrared spectrum, for sensing the near surface air temperature. For about half of the satellite pairs (N7-N8, N14-N15, N15-N16, and N16-N17), the variations of channel-7 bias across the observed temperature ranges are larger than 1 K. For other pairs of satellites with bias changes of less than 1 K, the variations are also notable.

***Channel 8*:** The bias values are generally within ±0.2 K for most of the satellite pairs, except for N6-N7, which has biases of around 0.4 K.

***Channel 9*:** The biases are mostly within ±0.4 K. The variations of the biases with temperature are relatively small compared to most of other sounding channels.

***Channel 10*:** Large bias values are observed for several satellite pairs. One of the contributing factors for the large biases can be traced to the spectral changes of channel 10 in the NOAA polar satellite series. The center frequency of channel 10 was near 1225 cm^{-1} for N6 to N10 and for N12, but changed to 796 cm^{-1} for N11 and N14, and to near 802 cm^{-1} for N15 and after. The figure also shows that the biases tend to be larger at low scene temperatures than at high temperatures.

***Channel 11*:** The biases are mostly within ±0.6 K. More than half of the satellite pairs have temperature dependent bias variations of larger than 0.5 K.

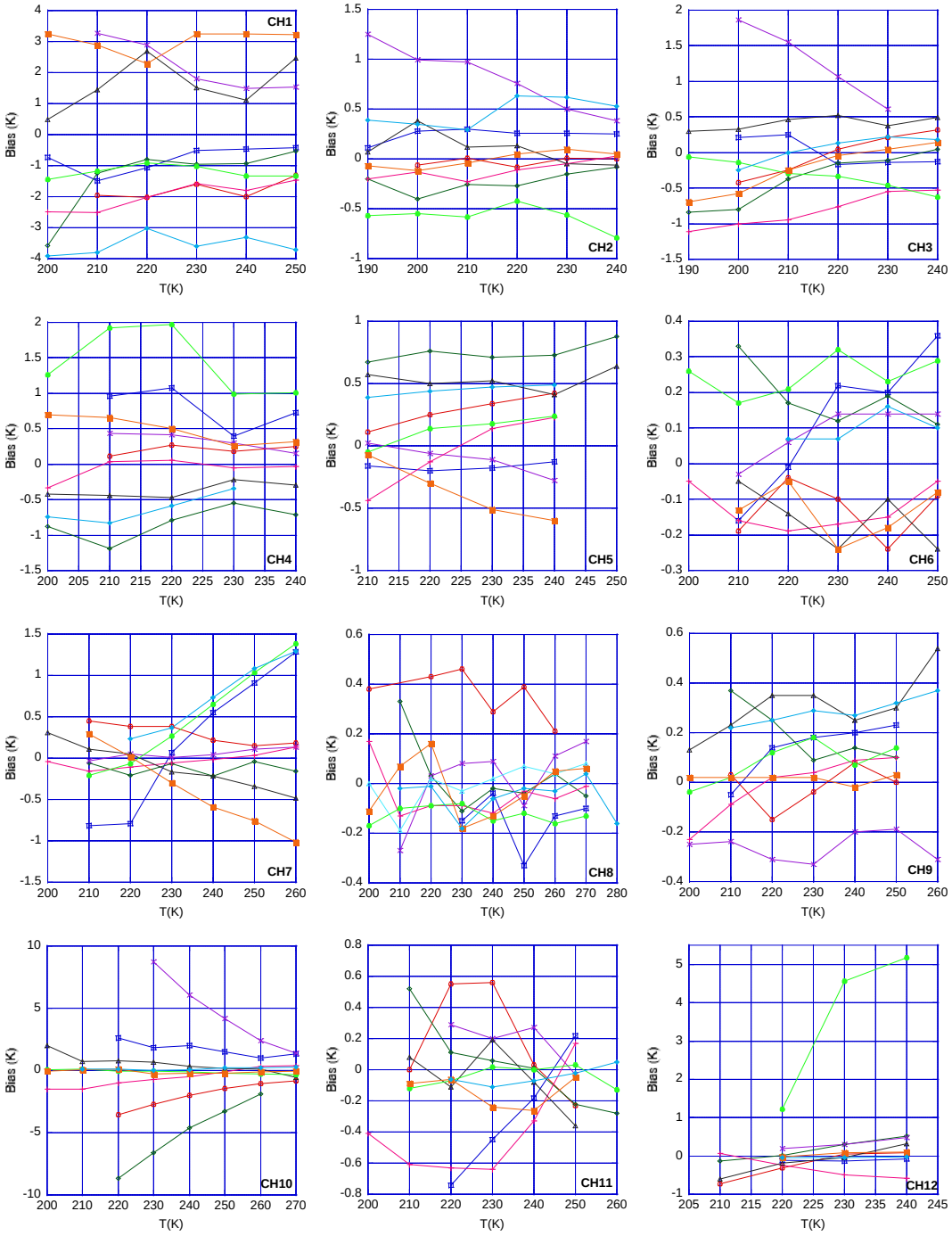

FIG. 1. Intersatellite biases of channels 1-12 for nine pairs of satellites based on SNO observations.

***Channel 12*:** The bias values are very large between N14 and N15. This is caused by the channel frequency change from about 1480 cm^{-1} on N14 and earlier satellites to 1530 cm^{-1} on the KLM series of satellites (N15 to N17). Due to the frequency change, the sensors on N14 and N15 essentially observed water vapor at different heights, which lead to the large bias of more than 5 K. For other satellite pairs, the biases are within the range of ±0.8 K. Many satellite pairs have bias variations of more than 0.5 K across the scene temperature ranges.

In the satellite time series, there is no overlap of observations between N8 and N9. There is only one month of overlap between N7 and N9, which is not long enough to provide sufficient intersatellite calibration data. To inter-calibrate and connect the satellites before N9, simulations from a radiative transfer model are used.

The HIRS data are first processed to remove cloudy pixels, and limb correction is applied (Jackson et al., 2003). The SNO observation spans a large range of the temperatures. However the measurement does not cover high temperature observations typically found in tropical regions. To estimate the intersatellite biases in low latitudes, a region with homogeneous temperature distribution, covering 20S-20N and 160W-100W, is selected for analysis. For the overlapping satellites, the differences of the regional monthly means are obtained. Examinations showed that the intersatellite biases for low latitudes follow the temperature dependant patterns established by the SNO measurements, with continuous increasing or decreasing patterns extending to high temperatures. Based on the intersatellite bias dataset, the HIRS channel brightness temperature data from individual satellites are adjusted to N12 as a base satellite using a similar data processing procedure described in Shi and Bates (2010).

3. TEMPERATURE AND HUMIDITY PROFILE RETRIEVAL

A neural network approach is applied to connect the relationship between the atmospheric profiles and the HIRS channel brightness temperatures. The profiles used to build a training dataset are obtained from a diverse sample of profiles simulated by the European Center for Medium-Range Weather Forecasts (ECMWF) system (Chevallier, 2001). These profiles are selected from the first and the 15th of each month between January 1992 and December 1993. The profiles are divided into seven groups differing by the total precipitable water vapor content of the profiles. About the same number of samples is extracted from each group, except for the group with the lowest precipitable water vapor content (0 to 0.5 $kg.m^{-2}$). For this group, twice as many profiles are extracted in consideration of the higher temperature variability from all types of situations from polar to tropics. The corresponding HIRS channel brightness temperatures are simulated by a radiative transfer model, RTTOV-9. The RTTOV is a broadband model in that the integration over the channel response is simulated directly. A description of the RTTOV can be found in Saunders et al. (1999). The RTTOV was one of the participating models in an intercomparison of HIRS and AMSU channel radiance computation (Garand et al., 2001). Among the selected seven HIRS channels (channels 2, 5, 9, 10, 11, 12, and 15) examined in the intercomparison, the standard deviations of RTTOV simulated radiances are within 0.55 K for channels 11 and 12 and within 0.25 K for the other channels.

Backpropagation neural networks similar to the approach used by Shi (2001) are used in developing the retrieval scheme. Different architectures with different numbers of layers and transfer functions are examined for the temperature and water vapor profiles retrieval. A three-layer network, with one input layer, one hidden layer, and one output layer, is chosen based on the performance compared to four-layer and five-layer networks. It is found that using a hyperbolic tangent function to propagate to the hidden layer and a logistic transfer function to propagate to the output layers gives the optimum network performance for the type of data studied. The definition of the hyperbolic tangent transfer function is

$$f(x) = \tanh(x), \quad (1)$$

and the definition of the logistic transfer function is

$$f(x) = \frac{1}{1+\exp(-x)}. \quad (2)$$

During the past thirty years the atmospheric CO_2 concentration increased substantially from 335 ppmv to nearly 390 ppmv. As the HIRS channel frequencies are located in the CO_2 band, the CO2 increase affects the HIRS measurement. To examine the CO_2 effect, RTTOV-9 is used to simulate HIRS brightness temperature with increasing CO_2. For each of the ECMWF sampled profiles, RTTOV-9 is run for the CO_2 concentration of 330 and 390 ppmv, respectively. The averaged brightness temperature of each HIRS channel is calculated. The differences of brightness temperatures between the two CO_2 concentration values are obtained. The simulation shows that when CO_2 concentration increases from 330 ppmv to 390 ppmv, for unchanged temperature profiles, the measurements from HIRS would appear to decrease in channels 3-7. The largest decreasing occurs in channel 6, with a value as large as 1.2 K. The decreases for channels 3, 4, 5, and 7 are 0.1, 0.9, 1.1, and 0.7 K, respectively. In channels sensing the stratosphere (channels 1 and 2), for the same profiles, the measurements from HIRS observation would appear larger in an increased CO2 environment. The increases in these two channels are 0.5 and 0.3 K, respectively. There are basically no impacts in channels 8-12, because these are window channel, ozone channel, and water vapor channels. As there are large effects from CO_2 increase on channels 1-7, if these effects are not considered in the temperature profile retrieval, it can lead to an underestimate of

tropospheric temperatures and an overestimate of stratospheric temperatures when CO_2 increases.

Therefore, the input set for the temperature and humidity profile retrievals include CO2 concentration in additional to the twelve HIRS longwave channels. The retrieved temperatures include surface skin temperature, temperature at 2 m, and temperatures at ten pressure levels from 1000 hPa to 50 hPa. The specific humidity values are obtained at 2 m and at seven levels from 1000 hPa to 300 hPa.

Only clear-sky profiles from the ECMWF sample profiles are used for building the training dataset. To take into account the effect of surface elevation, the clear-sky profiles are further divided into three groups according to their surface pressures. The first group contains profiles with surface pressures larger than 850 hPa. The second group has profiles with surface pressures between 850 and 700 hPa. And the remaining profiles with surface pressures less than 700 hPa are placed in the third group. For each of the groups, 20% are randomly extracted to construct a testing set, and another 20% are randomly extracted and set aside as a validation set for later statistical studies. A backpropagation network is trained by "supervised learning". The network is presented with a series of pattern pairs, each consisting of an input pattern and an output pattern, in random order until predetermined convergence criteria are met. At this time the network presents the input elements in the testing set and retrieves the output elements. Then the retrieved output elements are compared with the output elements in the testing set, and the averaged root mean square error (RMSE) of all the output elements is computed. The network parameters are saved if the averaged RMSE is less than that computed previously. This process is repeated until no improvement is found for a specified number of test trials.

The saved neural network parameters are applied to the data in the validation dataset. The RMSEs of temperature and specific humidity at all the levels are derived assuming the outputs in the validation database as truth data. For temperature, the RMSEs are 1.0 K for surface skin temperature, 2.2 K for 2 m temperature, 2.7 K for temperature at 1000 hPa, 1.3-1.5 K in the mid troposphere, and 2.0-2.6 K around the tropopause and in the lower stratosphere. For specific humidity, the RMSE is 1.9 g/kg at 2 m and 2.0 g/kg at 1000 hPa. It steadily decreases to 1.1 g/kg at 700 hPa and less than 0.4 g/kg above 500 hPa.

4. SUMMARY

An atmospheric temperature and humidity profile dataset is generated from intersatellite calibrated HIRS measurement onboard the NOAA polar satellites since 1979. To minimize the intersatellite biases, an intersatellite calibration is performed for three decades of HIRS measurement based on SNO observations. An algorithm is developed to account for the feature of varying biases with respect to brightness temperature. HIRS measurements from the NOAA series of polar orbiting satellites are calibrated to a baseline satellite to form a homogeneous database for deriving atmospheric temperature and humidity profiles. During the last thirty years, the atmospheric carbon dioxide concentration increased significantly. The increased carbon dioxide concentration has a large impact on the HIRS channel observations in the carbon dioxide band. The channels that are most affected by the carbon dioxide increase are the mid-atmosphere sensing channels such as channels 5 and 6. Simulation from RTTOV-9 shows that the increase in the carbon dioxide in the last thirty years can decrease the observation values of these two channels by more than 1.1 K. A neural network technique is applied to derive atmospheric temperature and humidity profiles that account for the observed carbon dioxide change over the last thirty years. Sampled profiles from ECMWF representing the global atmospheric conditions are used as the training dataset. The retrieval schemes are applied to inter-satellite calibrated HIRS measurement. The HIRS measurement provides uniformed coverage globally, including the vast ocean surface and remote mountainous regions that are often not covered by conventional radiosondes.

References:

Cao, C., M. Weinreb, and H. Xu, 2004: Predicting simultaneous nadir overpasses among polar-orbiting meteorological satellites for the intersatellite calibration of radiometers. *J. Atmos. Oceanic Technol.,* **21,** 537–542.

Cao, C., H. Xu, J. Sullivan, L. McMillin, P. Ciren, and Y.-T. Hou, 2005: Intersatellite radiance biases for the High Resolution Infrared Radiation Sounders (HIRS) onboard *NOAA-15, -16,* and *-17* from simultaneous nadir observations. *J. Atmos. Oceanic Technol.,* **22,** 381–395.

Chevallier, F., 2001: Sampled databases of 60-level atmospheric profiles from the ECMWF analyses. Research Report No. 4, EUMETSAT/ECMWF SAF programme.

Garand, L., D. S. Turner, M. Larocque, J. Bates, S. Boukabara, P. Brunel, F. Chevallier, G. Deblonde, R. Engelen, M. Hollingshead, D. Jackson, G. Jedlovec, J. Joiner, T. Kleespies, D. S. McKague, L. MaMillin, J.-L. Moncet, J. R. Pardo, P. L. Rayer, E. Salathe, R. Saunders, N. A. Scott, P. Van Delst, and H. Woolf, 2001: Radiance and Jacovian intercomparison of radiative transfer models applied to HIRS and AMSU channels. *J. Geophys. Res.*, **106**, 24017-24031.

Jackson, D. L., D. P. Wylie, and J. J. Bates, 2003: The HIRS Pathfinder radiance data set (1979-2001), paper presented at 12th Conference on Satellite Meteorology and Oceanography, Long Beach, California, February 10-13, 2003.

Saunders R.W., M. Matricardi and P. Brunel, 1999: An improved fast radiative transfer model for assimilation of satellite radiance observations, *Q. J. Royal Meteorol. Soc.*, **125**, 1407-1426.

Shi, L., 2001: Retrieval of atmospheric temperature profiles from AMSU-A measurement using a neural network approach. *J. Atmos. Ocean. Tech*., **18**, 340-347.

Shi, L., J. J. Bates, and C. Cao, 2008: Scene radiance-dependent intersatellite biases of HIRS longwave Channels. *J. Atmos. Oceanic. Technol.,* **25(12)**, 2219-2229.

Shi, L., and J. J. Bates, 2010: Three decades of intersatellite calibrated HIRS upper tropospheric water vapor. *J. Geophys. Res.,* in press.